[4]Th. Niemeijer, Physica (Utr.) **57**, 281 (1971).
[5]P. H. E. Meijer and D. J. O'Keefe, Phys. Rev. B **1**, 3786 (1970).
[6]M. Lax, J. Chem. Phys. **20**, 1351 (1951).
[7]D. Schiferl, J. Chem. Phys. **52**, 3234 (1970).

PHYSICAL REVIEW B VOLUME 7, NUMBER 5 1 MARCH 1973

Polarized-Neutron Study of the Induced Magnetic Moment in TmSb†

G. H. Lander and T. O. Brun
Argonne National Laboratory, Argonne, Illinois 60439

Oscar Vogt
Laboratorium fur Festkorperphysik, ETH, Zurich, Switzerland
(Received 11 October 1972)

The magnetic form factor of the induced moment in TmSb has been measured with polarized neutrons. Thulium antimonide is a singlet-ground-state system, i.e., it has no spontaneous magnetic moment, but under the conditions of the experiment the magnetization develops through the mixing of the ground state with the first excited state. The experiments were performed on a single crystal at 5 °K and an applied field of 12.5 kOe. Measurements were taken with $\vec{H} \parallel \langle 100 \rangle$ and $\vec{H} \parallel \langle 110 \rangle$. The theoretical magnetic form factor has been derived using the tensor-operator technique of Johnston, Lovesey, and Rimmer, and the nonrelativistic wave functions of Freeman and Watson. The experimental form factor with $\vec{H} \parallel \langle 100 \rangle$ is essentially a smooth curve as a function of $\sin\theta/\lambda$, while for $\vec{H} \parallel \langle 110 \rangle$ considerable anisotropy is observed at high scattering angles. This anisotropy arises from the nature of the ground state and is determined by the crystal field acting on the rare-earth ion. The present technique may therefore be useful in investigating the ground states of the many compounds with unquenched orbital moments and appreciable crystal field interactions. The experimentally observed anisotropy is in complete agreement with theory. Previous polarized-neutron experiments on rare-earth metals indicate that the spatial extent of the $4f$ electrons is more expanded than given by the nonrelativistic calculations. The observed form factor in TmSb does not agree with the form factor calculated with nonrelativistic wave functions. Good agreement is obtained by using the $4f$ radial distribution as determined from polarized-neutron measurements on thulium metal. A set of $\langle r^n \rangle$ integrals has been derived from the experimental radial densities.

I. INTRODUCTION

Over the last three years the polarized-neutron technique has been used successfully to measure the magnetic form factors of the heavy rare-earth metals gadolinium,[1] thulium,[2] and terbium.[3] These measurements indicate a major discrepancy between the experimentally deduced spatial density of the $4f$ electrons and that calculated with nonrelativistic wave functions.[4] The advent of relativistic calculations[5,6] appears to remove at least some of this discrepancy, although the problem of understanding the conduction-electron polarization still remains. In addition, measurements on the ionic system Gd_2O_3[1] indicate an unexpected agreement with the form factor derived from nonrelativistic wave functions. The rare-earth pnictides have been extensively studied recently, and the metallic compound TmSb (NaCl structure, $a_0 = 6.076$ Å) provides an excellent candidate for a polarized-neutron investigation for the following reasons: (a) Very accurate single-crystal magnetization experiments have been performed on TmSb by Cooper and Vogt,[7] and Foner *et al.*,[8] and used to derive the crystal field parameters. Additional magnetization experiments[7] on the $Tm_xY_{1-x}Sb$ system indicate that the exchange is negligible in TmSb. The results of Cooper and Vogt show that TmSb is a singlet-ground-state system, and that the induced moment at 4.2 °K is isotropic in fields less than 15 kOe. Inelastic-neutron measurements[9] have further refined the crystal field parameters, confirming the model proposed by Cooper and Vogt. (b) From an experimental point of view, TmSb is ideal for accurate form-factor measurements since a magnetic moment of $\sim 1\mu_B$ per Tm atom can be induced with a field ~ 10 kOe at helium temperature. (c) Polarized-beam measurements have been reported on thulium metal[2] and a comparison of the $4f$ electron wave functions in the two environments can be made.

The theoretical calculation of the magnetic form factor is also of interest since this is a singlet-ground-state system without exchange, and the form

factor should be capable of reflecting the mixing of the wave functions that characterizes the Van Vleck susceptibility. The first calculations by Trammell[10] of the magnetic form factor in the lanthanide series introduced the functions $\langle j_i \rangle$ and $\langle g_i \rangle$ relating to the spin and orbital parts of the magnetization density, respectively. An alternative method is the tensor-operator method proposed originally by Johnston,[11] and reviewed by Lovesey and Rimmer.[12] In the present experiment in which the electron configuration depends on the precise values of the crystal field parameters, the direction of the applied magnetic field, and the sample temperature, the power of the tensor method is particularly well illustrated. A brief account of the resulting "crystal field effects" has been published.[13]

The calculation of the magnetic cross section for TmSb is described in Sec. II. For the usual polarized-beam conditions, in which the scattering vector lies in the plane perpendicular to the applied magnetic field and direction of the neutron polarization, the magnetic form factor is a well defined quantity. The magnetic form factor at a scattering vector $\vec{\kappa}$ may be written

$$f(\vec{\kappa}) = \langle j_0 \rangle + c_2 \langle j_2 \rangle + c_4 \langle j_4 \rangle + c_6 \langle j_6 \rangle, \qquad (1)$$

where $\langle j_i \rangle$ are the radial integrals discussed in Sec. V, and c_2, c_4, and c_6 are coefficients defined by the electronic structure of the magnetic ion, which, in turn, is a function of the crystal field potential acting on the ion and the external conditions of applied magnetic field and temperature. These coefficients are calculated in Sec. II. The experimental details are given in Sec. III. A very severe extinction problem was encountered in the single crystal of TmSb (this difficulty caused the experiment to be abandoned two years ago), and the corrections applied are described in Sec. IV, along with the experimental results. The derivation of the $\langle j_i \rangle$ radial integrals is discussed in Sec. V. This section also contains a reanalysis of the polarized-beam measurements on thulium metal,[2] and a comparison between the $4f$-electron densities in the metal and the antimonide. The conclusions and possible extensions of the present work are summarized in Sec. VI.

II. THEORY

To calculate the elastic magnetic scattering cross section for TmSb we have used the tensor-operator method.[11,12] The conditions under which this method is advantageous are that (a) the unpaired electrons all belong to the same shell, (b) the electronic configuration of the ion is spectroscopically well characterized, and (c) the magnetization density is well localized. Clearly all these conditions are fulfilled in the case of the Tm^{3+} ion in TmSb. The triply ionized thulium ion has 12 well-localized $4f$ electrons, with a spectroscopic ground state designated by $^3H_6$. The crystal field potential acting on the free-ion wave functions is extremely well known from other work,[7–9] and the exchange interaction is negligible. In accordance with magnetization experiments on TmSb, and indeed on all rare-earth pnictides and chalcogenides, we assume that the magnetic moment arises entirely from the unpaired $4f$ electrons. The tensor-operator method, with particular reference to the rare-earth metals themselves, has been discussed by Balcar *et al.*,[14] and the present authors.[15] The extension to include crystal field effects is quite straightforward. However, the formulas appear at first sight rather formidable and, since no detailed calculations (or experimental measurements) of the magnetic form factor in similar compounds has been published, we have considered the derivation in some detail. To give an over-all view of the calculation we have started from the final formula, which is the well-known expression for the magnetic elastic scattering of polarized neutrons. Computational details are omitted but certain parts of the derivation, in particular, the relationship between the symmetry of the wave functions under the operation of the crystal field potential and the final terms in the cross section, are discussed in detail.

The elastic magnetic cross section for a neutron beam with polarization $\vec{P}$ scattered from an ion with a nuclear scattering length b is given by

$$d\sigma/d\Omega \propto b^2 - b\vec{P}\cdot\vec{E} + \tfrac{1}{4}\vec{E}\cdot\vec{E}. \qquad \text{(LR 7.14)} \quad (2)$$

(Equation numbers preceded by LR refer to those in Lovesey and Rimmer.[12]) The magnetic scattering length is defined as a vector $\vec{E}$, with spherical components E_Q given by

$$(2\pi\hbar^2/m)\, E_Q = \langle \psi_e | T_Q^1(e) | \psi_e \rangle, \qquad \text{(LR 7.5)} \quad (3)$$

where the electron wave functions are represented by ψ_e, and $T_Q^1(e)$ defines a tensor operator. The polarized-beam cross section is often expressed as

$$d\sigma/d\Omega \propto b^2 + 2bpPq^2 + q^2p^2, \qquad (4)$$

where p is the magnetic scattering amplitude and

$$\vec{q} = \hat{\kappa} \times (\hat{\eta} \times \hat{\kappa}),$$

where $\hat{\eta}$ and $\hat{\kappa}$ are unit vectors in the direction of the magnetic moment and scattering vector, respectively. The amplitude p is defined as

$$p = (0.2696 \times 10^{-12})\, \mu f(\hat{\kappa}) \text{ cm},$$

where μ is the magnetic moment in Bohr magnetons, and $f(\hat{\kappa})$ the magnetic form factor. Equation (4) was originally derived in the absence of orbital moment; however, the same structure may still

be valid even with the orbitial moment present. If we consider the neutron polarization parallel to the magnetic moment then Eq. (2) becomes

$$d\sigma/d\Omega \propto b^2 - bP E_0 + \tfrac{1}{4}(E_0^2 - 2E_{-1}E_1) \qquad (5)$$

and has the same structure as (4) only if $E_{-1}E_1 = 0$. This condition is fulfilled when the scattering vector is perpendicular to the magnetic moment (i.e., $q^2 = 1$). In the present experiment the majority of measurements do therefore have a form factor that may be separated out of Eq. (2). The special case of the upper-layer reflections ($q^2 \neq 1$) requires the evaluation of the terms E_{-1} and E_1 and, in principle, the measured polarization ratio R of the two neutron spin states rather than the form factor should be compared with that calculated.[14] For TmSb, however, Eq. (4) may be written

$$d\sigma/d\Omega \propto b^2 + 2bpPq^2 + q^2p^2 + q^2(1-q^2)\,\Delta p^2.$$

The additional terms Δp are very small so that the concept of a form factor is still useful.

The tensor operator $T_Q^K(e)$ is defined by

$$\langle \psi_e | T_Q^K(e, \vec{\kappa}) | \psi_e \rangle = \delta_{K,1}(4\pi\hbar^2/m)(0.54\times 10^{-12}) \sum_{K''Q''} (4\pi)^{1/2} Y_{Q''}^{K''}(\hat{\kappa}) \times \sum_{K'Q'} \Big[\sum_{\substack{\theta JM \\ \theta' J' M'}} \langle \theta' J' M' | \psi_e \rangle \langle \psi_e | \theta JM \rangle \{A(K'', K') + B(K'', K')\} \langle K'Q'J'M' | JM \rangle \Big] \langle K''Q''K'Q' | KQ \rangle. \quad \text{(LR 4.60)} \qquad (6)$$

This expression, although complicated, may be simplified and handled in stages for TmSb to illustrate the requirements of the calculation. First, note that the cross section is expressed in terms of spherical harmonics $Y_{Q''}^{K''}(\hat{\kappa})$. The essential part of the calculation is contained in brackets [ ] in Eq. (6). Fortunately this summation is simplified if only one SLJ manifold is being considered (as in TmSb) and the term becomes

$$\sum_{M,M'} \langle JM' | \psi_e \rangle \langle \psi_e | JM \rangle \{A(K'', K') + B(K'', K')\} \times \langle K'Q'JM' | JM \rangle. \qquad (7)$$

To perform the sum over M and M' all coefficients of the wave-function expansion $|\psi_e\rangle = \sum_i a_i |JM_i\rangle$ must be known. The terms $A(K'', K')$ and $B(K'', K')$ are discussed fully in Lovesey and Rimmer[12] (Sec. 5) and coefficients related to these terms are tabulated in Refs. 14 and 15, although not in quite the same form. These parameters depend on the f-electron configuration in the free ion, as well as on the radial part of the one-electron wave functions through the integrals $\langle j_i \rangle$. The A and B terms correspond to the orbital and spin parts of the magnetic interaction with the neutron, respectively. As discussed in Ref. 15 the spatial dependence of the wave functions, i.e., the dependence on $\langle j_i \rangle$, may be separated out in evaluating the A and B terms. For example $A(K'', K') = A'(K'', K')\{\langle j_{K'+1} \rangle + \langle j_{K'-1} \rangle\}$, where the $A'(K'', K')$ are independent of the $\langle j_i \rangle$ integrals. The problem remaining before Eq. (6) can be programmed is to obtain the complete wave functions ψ_e of the crystal field states. Each of the ψ_e states must then be treated as in (7), and the ensemble average $\langle T_Q^K \rangle$ calculated according to the population of each level.

The Hamiltonian $\mathcal{H}$ for an ion placed in a crystal may be written

$$\mathcal{H} = \mathcal{H}_F + V,$$

where $\mathcal{H}_F$ is the Hamiltonian of the free ion and V is the crystal field potential. In calculating the magnetic properties, or the neutron scattering cross section, an extremely good approximation for most of the lanthanide ions is to consider only the effect of V on the ground state of the free ion. The effect of this potential on the rare-earth ions in a cubic field has been analyzed by Lea, Leask, and Wolf[16] (LLW), and Hutchings.[17] LLW have introduced two parameters W and x, where W gives the absolute value of the crystal field energy levels, and x is related to the ratio of the fourth- to sixth-order terms, and are the only two independent parameters for a field with cubic symmetry. Although W and x have been used widely, they are not the most convenient parameters, especially in the framework of the tensor-operator method. Wybourne[18] has discussed this point and pointed out the advantages of expanding the potential V in terms of tensor operators $C_q^{(k)}$ such that

$$V = \sum_{k,q,i} B_q^k (C_q^{(k)})_i, \qquad (8)$$

where the summation involving i is over all the electrons of the ion, and

$$C_q^{(k)} = [4\pi/(2k+1)]^{1/2} Y_q^k,$$

where Y_q^k is the spherical harmonic operator. Specifically we require the coefficients B_q^k, and in the case of a cubic crystal with the quantization along the cube edge the only nonzero parameters are B_0^4, B_4^4, B_0^6, and B_4^6. These are related to the more familiar parameters A_m^n (see LLW) as follows:

$$B_0^4 = 8A_4^0\langle r^4\rangle, \quad B_4^4 = (\tfrac{20}{35}\sqrt{70})A_4^0\langle r^4\rangle,$$
$$B_0^6 = 16A_6^0\langle r^6\rangle, \quad B_4^6 = (-8\sqrt{14})A_6^0\langle r^6\rangle, \tag{9}$$

where the $\langle r^n\rangle$ are the radial expectation values of the $4f$ electron. The parameters A_m^n depend on the ionic environment. For an octahedral array of charges, as in TmSb, each of magnitude Z and at a distance R from the thulium ion,

$$A_4^0 = \tfrac{7}{16}Ze^2/R^5 \quad \text{and} \quad A_6^0 = \tfrac{3}{64}Ze^2/R^7. \tag{10}$$

The relationships between W and x and the parameters B_0^4 and B_0^6 are

$$B_0^4 = 8Wx/\beta F(4) \quad \text{and} \quad B_0^6 = 16W(1-|x|)/\gamma F(6), \tag{11}$$

where β, γ, $F(4)$, and $F(6)$ are defined in Lea, Leask, and Wolf.[16]

In calculating the neutron cross section it is convenient to choose the common direction of the applied magnetic field and the neutron polarization as the axis of quantization. The advantage in using the B_q^k's defined by Eq. (8) then becomes apparent, since the parameters for an arbitrary z axis can be obtained easily from the coefficients defined for the axis of quantization along a direction of high symmetry. The new coefficients $B_{q'}^{\prime k}$ are given by

$$B_{q'}^{\prime k} = \sum_{q=-k}^{k} B_q^k D_{q'q}^{(k)}(\alpha, \beta, \gamma), \tag{12}$$

where $D_{q'q}^{(k)}(\alpha, \beta, \gamma)$ are the rotation matrices for the Euler angles α, β, and γ. The problem of determining the rotation matrices is a standard one in quantum mechanics, and is treated elsewhere, e.g., Edmonds,[19] Marshall,[20] and Messiah.[21] The relationship between the various B_q^k for the three principal directions in a cubic system are given in Table I. The matrix elements of the crystal field interaction are given by

$$\langle JM|V|JM'\rangle = \sum_{kq} B_q^k \langle kqJM'|JM\rangle \frac{1}{(2J+1)^{1/2}}$$
$$\times (f^n \alpha SLJ\|U^{(k)}\|f^n \alpha SLJ)(f\|C^{(k)}\|f), \tag{13}$$

where the doubly reduced matrix elements may be obtained from Eq. (6.5) of Wybourne[18] and the tabulation by Nielsen and Koster.[22] The important part of this equation is the product $B_q^k\langle kqJM'|JM\rangle$. The Clebsch–Gordan coefficient is zero unless $q + M' - M = 0$, or $M - M' = \Delta M = q$, so this acts as a selection rule for the nonzero matrix elements. For example, in the $\langle 100\rangle$ direction the values of B_q^k have $q = 0$ and 4, so the off-diagonal terms in the final matrix must have $\Delta M = 4$. In the $\langle 100\rangle$ direction, however, $\Delta M = 2$. This feature of the crystal symmetry is important in the derivation of the magnetic form factor, and will be reflected in the final form of the cross section. The diagonalization of the resulting matrix gives the familiar crystal field energy levels and eigenfunctions published by Lea, Leask, and Wolf.[16] Following Cooper and Vogt[7] the effect of an externally applied magnetic field may be incorporated into the Hamiltonian by adding the diagonal matrix

$$\mathcal{H}_M = -g\mu_B HM\delta_{JM,JM'},$$

where g is the Landé splitting factor and H the magnitude of the magnetic field. The magnetization at a field H and temperature T is calculated from the eigenvalues and eigenfunctions of the Hamiltonian including the magnetic field,

$$\mathfrak{M} = g\,\mathrm{Tr}[Me^{-\mathcal{H}/kT}]/\mathrm{Tr}[e^{-\mathcal{H}/kT}]. \tag{14}$$

To obtain numerical results requires the values of B_0^4 and B_0^6, or equivalently W and x. In TmSb the induced moment at low temperature and field depends only on the splitting between the Γ_1 ground state and the first excited state of the Γ_4 triplet [see Eq. (2.10) of Ref. 7]. This splitting, ΔT, is given by Cooper and Vogt as 26.6 °K, corresponding to a value of $W = -0.887$ °K. The inelastic-neutron experiments[9] give $\Delta T = 25.8 \pm 0.2$ °K ($W = -0.993$ °K). The various determinations of of W and x are discussed by Foner *et al.*,[8] who point out that while magnetization measurements define x as lying within the range -0.6 to -1.0, inelastic-neutron-scattering experiments define this parameter much more closely as $x = -0.785 \pm 0.02$. Although the elastic magnetic cross section is sensitive to ΔT, which essentially defines the magnetic moment for a given field, the form factor for TmSb at 4.2 °K (i.e., the κ dependence of the cross section) is insensitive to the magnetic moment over a relatively wide range of applied field. Similarly the variation of the form factor with the parameter x is evident only at much higher fields than are currently available. The choice of W and x is therefore not particularly critical to

TABLE I. The normalized B_q^k parameters for the three principal directions in a cubic crystal system as defined in Eq. (8).

	⟨100⟩	⟨110⟩	⟨111⟩
B_0^4	1.0000	−0.2500	−0.6667
B_2^4		0.7906	
B_3^4			0.7968
B_4^4	0.5976	0.4482	
B_0^6	1.0000	−1.6250	1.7778
B_2^6		−0.6404	
B_3^6			1.0734
B_4^6	−1.8708	1.1693	
B_6^6		−0.9500	1.1257

this experiment, and we have used

$$\Delta T = 26.0\ ^\circ\mathrm{K}\ (W = 1.015\ ^\circ\mathrm{K}) \tag{15}$$

and

$$x = -0.80,$$

which are compatible with previous experiments. In the ⟨100⟩ direction the parameters B_0^4 and B_0^6 are then given by Eq. (11) as

$$B_0^4 = 663.2\ ^\circ\mathrm{K} \quad \text{and} \quad B_0^6 = 76.64\ ^\circ\mathrm{K}. \tag{16}$$

If the quantization is along the cube axis the ground-state wave function in zero field is

$$|\psi\rangle_{100}(H=0) = 0.6614|4\rangle - 0.3536|0\rangle + 0.6614|-4\rangle, \tag{17}$$

where the ket $|JM\rangle$ has been written as $|M\rangle$. This is the Γ_1 singlet, and clearly has no magnetic moment. On applying a magnetic field a moment is induced on the ion because the ground state becomes a mixture of the Γ_1 and Γ_4 states. At 5 °K the contribution to the low-field magnetization from the Γ_4 state alone is negligible because the splitting ΔT is much larger than the temperature. With an applied field of 12.5 kOe, the magnitude used in the experiment, the ground-state wave function becomes

$$|\psi\rangle_{100}(H=12.5) = 0.7526|4\rangle - 0.3493|0\rangle + 0.5581|-4\rangle. \tag{18a}$$

Similarly the ground states with the field applied along the other two directions are

$$|\psi\rangle_{100}(H=12.5) = 0.4114|6\rangle - 0.4718|4\rangle + 0.2392|2\rangle + 0.5637|0\rangle + 0.2059|-2\rangle - 0.3494|-4\rangle + 0.2621|-6\rangle \tag{18b}$$

and

$$|\psi\rangle_{111}(H=12.5) = 0.4884|6\rangle + 0.4167|3\rangle + 0.6170|0\rangle - 0.3324|-3\rangle + 0.3110|-6\rangle. \tag{18c}$$

The quantization axis is chosen parallel to the field in each case. At low fields the induced moment in a cubic system is independent of the direction of the applied field (see Fig. 6 of Cooper and Vogt),[7] and we are essentially within this region. With $H = 12.5$ kOe the induced moment per thulium ion is $1.18\mu_B$ for $\vec{H}\parallel\langle 100\rangle$, $1.19\mu_B$ for $\vec{H}\parallel\langle 110\rangle$, and $1.20\mu_B$ for $\vec{H}\parallel\langle 111\rangle$. The structure of these wave functions, i.e., the $|M\rangle$ values involved, may be traced directly to the nonzero coefficients for that field direction in Table I.

Returning to Eq. (7), the Clebsch–Gordan $\langle K'Q'JM'|JM\rangle$ is zero unless $Q' = M - M' = \Delta M$, and the previous restrictions on ΔM indicate that the minimum values of $|Q'|$ are 4, 3, and 2 depending on whether the applied field is parallel to ⟨100⟩, ⟨111⟩, or ⟨110⟩, respectively. The majority of measurements in the present experiment have been taken with the scattering vector perpendicular to the applied field so that only the term with $Q = 0$ in Eq. (6) will be discussed. The final Clebsch–Gordan in Eq. (6) then implies $Q'' + Q' = 0$. The magnetic form factor is expressed in terms of spherical harmonics $Y_{Q''}^{K''}(\Theta, \Phi)$, where the angles Θ and Φ define the direction of the scattering vector. Terms with $Q'' = 0$ have no Φ dependence; i.e., the value of the term depends only on the angle Θ between the moment direction and the scattering vector, in this discussion $\frac{1}{2}\pi$. The order of the radial functions $\langle j_i\rangle$ involved in any particular term is defined by the parameter K' in $A(K'', K') + B(K'', K')$. Terms including $\langle j_2\rangle$ require $K' = 1$ or 3, $\langle j_4\rangle$ require $K' = 3$ or 5, etc. For the ⟨100⟩ direction the minimum nonzero value of $|Q''|$ and $|Q'|$ (and hence K'' and K') is 4. The first term that appears with a Φ dependence is therefore of the form $Y_4^4(\frac{1}{2}\pi, \Phi)\langle j_4\rangle$. This, of course, reflects the basic fourfold symmetry when the crystal is viewed along the cube axis. Similarly for the ⟨111⟩ and ⟨110⟩ directions the leading terms containing the Φ dependence are $Y_3^4(\frac{1}{2}\pi, \Phi)\langle j_2\rangle$ and $Y_2^2(\frac{1}{2}\pi, \Phi)\langle j_2\rangle$, respectively. The value of $Y_3^4(\frac{1}{2}\pi, \Phi)$ is zero, and for the ⟨111⟩ direction the first nonzero term is $Y_6^6(\frac{1}{2}\pi, \Phi)\langle j_6\rangle$. As discussed in Sec. V, for $\sin\theta/\lambda < 1.0$ Å^{-1}, the $\langle j_i\rangle$ functions for $i > 0$ rapidly diminish in magnitude with increasing order, and anisotropies involving $\langle j_4\rangle$ and $\langle j_6\rangle$ are very hard to observe experimentally. The result, therefore, is that of the three principal directions reasonable anisotropies should be observed only with the field applied parallel to the ⟨110⟩ direction. The experimental results on TmSb fully confirm this expectation. We should emphasize that the effects observed are a direct consequence of the crystal field potential. In the fully ordered heavy rare-earth metals, for example, the wave functions are described by the single state $M = J$, which gives the maximum possible magnetic moment using Hunds rule and Russell–Saunders coupling. Clearly for this situation no cross terms appear in Eq. (7), i.e., $\Delta M = 0$, and the final cross section is composed of terms in $Y_0^{K''}$, which do not include any Φ anisotropy [see, for example, Eq. (8.20) of Lovesey and Rimmer]. The coefficients of the various terms in $Y_{Q''}^{K''}(\Theta, \Phi)$ and $\langle j_i\rangle$ are, of course, only found after the evaluation of Eq. (6). These are given in Table II.

III. EXPERIMENTAL

All experiments were performed on a single crystal with dimensions of $4.7 \times 2.3 \times 0.8$ mm, with all faces being (100) planes. For the first series of measurements ($\vec{H}\parallel\langle 100\rangle$), the field was applied parallel to the long axis of the crystal. During the remounting of the crystal (for $\vec{H}\parallel\langle 110\rangle$) a small portion of the crystal was lost, reducing the long

TABLE II. Coefficients for the magnetic cross section ($Q=0$ term only) for TmSb with the sample temperature $T=5$ °K and the magnetic field of 12.5 kOe applied in the ⟨100⟩ and ⟨110⟩ directions. The coefficients modify terms $Y_{Q''}^{K''}(\Theta,\Phi)\langle j_l\rangle$, where Θ and Φ are defined by the scattering vector and the field direction, and $\langle j_l\rangle$ are the radial integrals (see Sec. V).

		$\vec{H}\parallel\langle 100\rangle$				$\vec{H}\parallel\langle 110\rangle$			
K''	Q''	$\langle j_0\rangle$	$\langle j_2\rangle$	$\langle j_4\rangle$	$\langle j_6\rangle$	$\langle j_0\rangle$	$\langle j_2\rangle$	$\langle j_4\rangle$	$\langle j_6\rangle$
0	0	0.3922	0.2615			0.3978	0.2652		
2	0	−0.1754	−0.1344	−0.0064		−0.1779	−0.1140	0.0017	
2	2						−0.0090	−0.0033	
4	0		0.0130	0.0246	0.0031		−0.0034	−0.0046	−0.0005
4	2						0.0078	0.0177	0.0023
4	4			0.0055	0.0009			0.0027	0.0004
6	0			−0.0165	−0.0259			0.0028	−0.0109
6	2							−0.0127	0.0039
6	4			−0.0057	−0.0057			−0.0028	−0.0105
6	6								−0.0040
8	0				0.0205				0.0099
8	2								−0.0051
8	4				0.0045				0.0093
8	6								0.0045

dimension to 3.4 mm. The field was applied at 45° to the long axis.

Before starting the polarized-beam experiments the intensities of four octants of Bragg reflections with $\sin\theta/\lambda \le 0.77$ Å^{-1} were measured at room temperature with a four-circle diffractometer ($\lambda = 1.05$ Å) at the CP-5 Research Reactor. These measurements indicated a large amount of extinction, i.e., the intensities of the strong reflections were reduced in value relative to weaker reflections. However, attempts to account for the extinction were judged successful (see Sec. IV), and the crystal was therefore transferred to the polarized-neutron diffractometer ($\lambda = 1.05$ Å), also located at the CP-5 Research Reactor.

The polarized-beam technique yields, in principle, the so-called flipping ratio

$$R = (1+\gamma)^2/(1-\gamma)^2, \tag{19}$$

where $\gamma = M/N$, and M and N are the magnetic and nuclear structure factors, respectively. TmSb has the NaCl-type crystal structure and only two structure factors are present, for hkl all even, $N_+ = b_{Tm} + b_{Sb}$, and for hkl all odd, $N_- = b_{Tm} - b_{Sb}$, where b_{Tm} and b_{Sb} are the scattering amplitudes of thulium and antimony, respectively. The magnetic structure factor has the same form for all reflections and is given by $M = p_0 \mu f(\vec{\kappa})$, where p_0 is the constant 0.2696×10^{-12} cm, μ is the magnetic moment per thulium ion in Bohr magnetons, and $f(\vec{\kappa})$ is the form factor. In practice Eq. (19) has to be modified due to incomplete incident polarization and imperfect spin reversal. In the present experiment both the neutron polarization and flipping efficiency were 0.992 ± 0.003, and the resulting small corrections have been made in all cases, although they are normally less than 2%. Other sources of possible error arise from neutron depolarization, half-wavelength contamination, multiple scattering effects, and extinction. Neutron depolarization has been neglected since TmSb is an isotropic paramagnet. Half-wavelength contamination was important for the weak reflections (hkl odd), and flipping-ratio measurements were made with a ^{239}Pu filter in the incident neutron beam; this reduces the contamination of the $\frac{1}{2}\lambda$ component by a factor of 50. Multiple scattering effects are difficult to eliminate totally, but the good agreement between flipping ratios measured on equivalent reflections gives confidence that these effects are small, or at least negligible compared to the extinction. For a number of reflections the flipping ratio was examined as a function of the crystal-setting angle, i.e., measured as the crystal was swept through a rocking curve, and in no cases was any variation of the flipping ratio observed.

An examination of Eq. (19) and the values of γ involved indicates that for the parameters $\mu = 1.2\mu_B$ per Tm ion, $b_{Tm} = 0.72\times10^{-12}$ cm,[23] and $b_{Sb} = 0.564\times10^{-12}$ cm,[24] $\gamma = 0.25 f(\vec{\kappa})$ for even hkl, and $\gamma = 2.1 f(\vec{\kappa})$ for odd hkl. The polarized-beam method is particularly sensitive for $\gamma < 0.7$, when the instrumental corrections, except extinction, are relatively unimportant. The majority of measurements were made on the strong reflections (hkl even), and only a few of the low-angle odd reflections were measured. These are weak, e.g., the spin-down intensity of the (111) reflection with the Pu filter inserted was ~40 counts/min on top of a background count of ~10 counts/min, and are very sensitive to the quantity $|b_{Tm} - b_{Sb}|$. In fact, together with the unpolarized-neutron results, our measurements define this difference, and hence b_{Tm} relative to b_{Sb}, exceedingly well.

All measurements were made at helium temperature in a magnet assembly with an applied field of ~13 kOe. Figure 1 gives the theoretical variation with temperature of the magnetic moment (assuming a constant applied field). The choice of crystal field parameters, W and x is discussed in Sec. II, and is compatible with previous experiments.[7-9] Such a moment behavior is implied from Fig. 3 of Cooper and Vogt,[7] and indicates the singlet-ground-state nature of the Tm ion. Figure 1 also illustrates the importance of keeping the temperature below ~5 °K if the induced magnetic moment is to be truly temperature independent. Using a carbon resistor in contact with the sample, variations of temperature between 4.2 and 5.4 °K were measured, implying a variation of ±0.8% from the mean value of the magnetic moment. The applied magnetic field was constant (<0.2% variation) throughout the experiment, and was measured with a Hall probe as 12.5 kOe. Unfortunately the Hall probe samples a larger area in the plane perpendicular to the field than the crystal and, as a result, the field measured with the Hall probe is a lower limit; the applied field is estimated to be in the region of 12.5–13.0 kOe. Small demagnetization effects are expected to reduce the magnitude of the effective field by ~200 Oe in the case of the symmetrical situation with $\vec{H}\|\langle 100\rangle$, and ~300 Oe when $\vec{H}\|\langle 110\rangle$.

IV. RESULTS

Extinction

The problem of extinction in single crystals has been treated in detail by Zachariasen,[25] and it appears from numerous reported structure refinements using both x-ray and neutron diffraction that this method gives a reliable correction for extinction. Modifications to include anisotropic effects[26] and severe extinction in neutron diffraction[27] have also been made, but are not included in this paper. The basic Zachariasen formula for the neutron case may be written

$$I_{\text{obs}}/I_c = y = 1/(1+2gQ\bar{t})^{1/2}, \tag{20}$$

where I_{obs} and I_c are the observed and calculated intensities, $\bar{t}$ is the effective path length through the crystal, g is the extinction parameter, and Q is the crystallographic reflectivity given by $Q = \lambda^3 |F_c|^2/(V^2 \sin 2\theta)$, where F_c is the calculated structure factor, V is the volume of the unit cell, and θ is the Bragg angle. Equation (20) represents a simplification of the Zachariasen formula, since it assumes that extinction is either type I or type II (see Ref. 25 for a discussion of these terms). We believe type-II extinction to be the more likely in view of the relatively severe extinction found (y parameters as low as 0.6). In this case g is proportional to the mean radius r of small perfect domains in the crystal ($g = r/\lambda$), and the degree of extinction is not related to the mosaic spread of the crystal. Changing the mosaic spread, even if possible for such a brittle material as TmSb, would have little, if any, effect on the extinction. The observed rocking curves were board (full width at half-maximum greater than the experimental resolution) and showed considerable structure, but the flipping ratio was independent of the rocking angle, as expected for the type-II extinction.

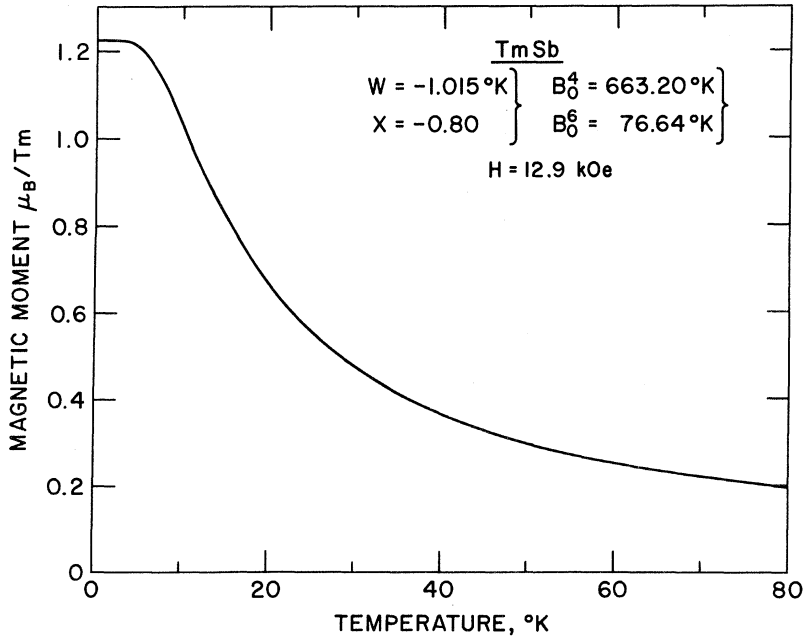

FIG. 1. Temperature dependence of the magnetic moment in TmSb with an applied field of 12.9 kOe. The crystal field parameters B_0^4 and B_0^6 (or equivalently W and x) are discussed in the text.

The shape of the TmSb crystal in the present experiment is particularly suitable for examining extinction effects, since the path lengths $\bar{t}$ differ by up to a factor of 3 for equivalent reflections. The path lengths were calculated using a standard crystallographic absorption program with an absorption coefficient of 1.29 cm^{-1}. After correcting for regular absorption the unpolarized-neutron results were refined with a least-squares routine that incorporated the Zachariasen correction. The weak reflections (*hkl* odd) were not included in this refinement. An isotropic temperature factor of 0.55 $Å^{-2}$, corresponding approximately to a Debye Θ of 210 °K,[28] and scattering amplitudes of 0.72×10^{-12} and 0.564×10^{-12} cm for thulium and antimony, respectively, were used. This refinement of 251 measured reflections with two adjustable parameters, an over-all scale factor S, and the extinction parameter g, resulted in a residual R $(=\sum||F_{obs}| - |F_c||/\sum|F_c|$, where F_{obs} and F_c are the observed and calculated structure factors, respectively) of 0.014. The value for g was 2660 ± 150, and the correlation between g and S was 0.93. A representative sample of the calculated and observed structure factors and the y values for each reflection is given in Table III. By comparing the intensities of the weak (*hkl* odd) and strong (*hkl* even) reflections the ratio $|b_{Tm}-b_{Sb}|/|b_{Tm}+b_{Sb}| = 0.114\pm0.003$. Assuming $b_{Sb}=(0.564\pm0.001)\times10^{-12}$ cm[24] the value of b_{Tm} determined from this ratio is $(0.708\pm0.005)\times10^{-12}$ cm. Values published for b_{Tm} are $(0.69\pm0.02)\times10^{-12}$ cm[29] and $(0.720\pm0.006)\times10^{-12}$ cm.[23] Our determination of b_{Tm} assumes the sample is stoichiometric. Any departure from stoichiometry in the rare-earth pnictides is expected to result in vacancies at the anion sites. We have no reason to expect anion vacancies in the present sample but, if present, the b_{Tm} deduced from our measurements would be lower than 0.708×10^{-12} cm.

TABLE III. Representative results of the least-squares refinement of the unpolarized study of the TmSb crystal. $\bar{t}$ is the path length, F_c is the calculated structure factor, y is the reduction in intensity calculated from the refined extinction parameter ($g=2660\pm150$), F_{obs} is the observed structure factor, and S is the refined scale factor (27.2 ± 0.1). 251 reflections were used in the refinement and an isotropic temperature factor of 0.55 $Å^{-2}$ was used.

hkl	2θ	$\bar{t}$ (cm)	F_c (10^{-12} cm)	y	F_{obs}/S	$F_c y^{1/2}$
020	19.95	0.187	5.060	0.61	3.95	3.94
$0\bar{2}0$		0.188		0.61	3.97	3.94
200		0.079		0.76	4.21	4.41
$\bar{2}00$		0.080		0.76	4.26	4.41
002		0.145		0.65	4.28	4.09
222	34.91	0.105	4.912	0.81	4.39	4.41
$2\bar{2}2$		0.104		0.81	4.31	4.41
$\bar{2}22$		0.105		0.81	4.41	4.41
$\bar{2}\bar{2}2$		0.105		0.81	4.28	4.41
240	45.57	0.149	4.774	0.80	4.24	4.25
420		0.092		0.86	4.33	4.42
042		0.148		0.80	4.28	4.25
402		0.082		0.87	4.41	4.45
024		0.185		0.76	4.25	4.16
204		0.082		0.87	4.49	4.45
482	105.05	0.104	3.756	0.92	3.64	3.60
842		0.129		0.90	3.62	3.57
284		0.098		0.92	3.61	3.61
824		0.114		0.91	3.64	3.59
248		0.168		0.88	3.60	3.52
428		0.128		0.90	3.75	3.57

For experiments measuring magnetic as well as nuclear elastic scattering, the reflectivity Q in Eq. (20) has to include both the nuclear and magnetic structure factors, N and M, respectively. In the special case of polarized neutrons and measurements made in a plane perpendicular to both the direction of the magnetic moment and neutron spin (as are the majority of the present measurements) Q^+ contains the term $|N+M|^2$ and Q^- the term $|N-M|^2$. Clearly two different extinction corrections y^+ and y^- are needed to correct the intensities measured in the two spin states, and

$$R_{obs}=\frac{I^+_{obs}}{I^-_{obs}}=\frac{I^+_c}{I^-_c}\,\frac{y^+}{y^-}=R_{corr}\left(\frac{1+2gQ^-\bar{t}}{1+2gQ^+\bar{t}}\right)^{1/2}, \qquad (21)$$

where R_{obs} is the observed flipping ratio and R_{corr} the flipping ratio in the absence of extinction. Equation (21) has also to be modified for certain instrumental effects but, although they were considered in processing the data, they have been omitted for the sake of clarity in this discussion. Such effects are very small in the present experiment. We have defined an apparent ratio γ_{obs} and a corrected ratio γ_{corr} from Eq. (19) using R_{obs} and R_{corr}, respectively. Unfortunately Eq. (21) cannot be solved directly for γ_{corr}, since the quantities Q^+ and Q^- also contain M and N, and hence γ_{corr}, but the equation may be solved readily by an iterative procedure. As an example of the extinction effects consider the (200) and (020) reflections as measured with $\vec{H}\parallel[001]$. For both reflections $Q^+=2.69\times10^{-3}$ cm and $Q^-=1.04\times10^{-3}$ cm. Assuming $g=2500$ for the (200) with $\bar{t}=0.079$ cm, then $y^+=0.70$ and $y^-=0.84$. The ratio R_{obs}/R_{corr} is then 0.827; for the (020), with $\bar{t}=0.187$ cm, this ratio is 0.749. The errors arising from neglecting extinction are therefore very appreciable, in some cases exceeding 20%. Since the flipping ratio can be measured easily to an accuracy of 1%, the extinction correction must be known accurately if the full power of the polarized-beam technique is to be utilized. A common method used for investigating the degree of extinction is to vary the incident neutron wavelength. Consider, for example, the incident wavelength reduced from 1.05 to 0.85 Å. The re-

flectivities are then reduced, so that $Q^+ = 1.76 \times 10^{-3}$ cm and $Q^- = 0.68 \times 10^{-3}$ cm. If g, the extinction parameter, is assumed constant at 2500, then for the (200) $y^+ = 0.77$ and $y^- = 0.89$, with a ratio of 0.865. Thus, although the extinction on the strong spin-up intensity is decreased by ~10%, the correction to the flipping ratio is decreased by only 4%, and is still a sizable 14%. In practice the situation is likely to be worse, since with type-II extinction[25] the parameter g is inversely proportional to the wavelength, and by decreasing the wavelength to 0.85 Å we expect g to increase to ~3100. For the same reflection, R_{obs}/R_{corr} would then be 0.846 for $\lambda = 0.85$ Å, compared to 0.827 for $\lambda = 1.05$ Å. Clearly no advantage would be gained by reducing the neutron wavelength. As an alternative we have looked for consistency between equivalent reflections with different path lengths as a judge of the reliability of the extinction correction This is illustrated in Table IV, in which the values of γ_{corr} calculated with three different values of g are tabulated. The agreement between equivalent reflections is good provided that g is in the range 2000–3000. Changing g in this range acts very much like a scale factor on all reflections, but any other value of g fails to give agreement. The column γ_{obs} corresponds to $g = 0$ (i.e., assuming no extinction) and for this value of g the differences in the {200} and {400} equivalences are very marked. A g value of 2500 has been chosen as this gives the best agreement with the absolute value of the magnetic scattering length, and is also consistent with the value of g derived from the unpolarized-neutron experiments.

Experimental Results

The results for $\vec{H} \parallel [001]$ and $\vec{H} \parallel [0\bar{1}1]$ are given in Tables IV and V, respectively. With $\vec{H} \parallel [0\bar{1}1]$ no differences occur in the path lengths for equivalent reflections in the $(0\bar{1}1)$ plane. For some of these reflections the theoretical form factors are very nearly the same as for $\vec{H} \parallel [001]$, and in those cases good agreement between γ_{corr} for the two field directions is obtained using the g value of 2500.

In Table VI the weak (hkl odd) reflections are presented. With $\vec{H} \parallel \langle 100 \rangle$ none of these reflections

TABLE IV. Results for the polarized-beam measurements on TmSb with the field applied parallel to [001]. $\bar{t}$ is the path length, R_{obs} is the observed flipping ratio; γ_{obs} is derived from R_{obs} using an incident polarization and flipping efficiency of 0.992 ± 0.003. The corrected γ values are derived for different values of the extinction parameter g. The final column $(\mu f)_{corr}$ is derived using $g = 2500$, and with scattering lengths $b_{Tm} = 0.705 \times 10^{-12}$ cm and $b_{Sb} = 0.564 \times 10^{-12}$ cm.

hkl	$\frac{\sin\theta}{\lambda}$	$\bar{t}$ (cm)	R_{obs}	γ_{obs}	corrected γ $g=2000$	$g=2500$	$g=3000$	$(\mu f)_{corr}$ (μ_B)
200	0.165	0.079	2.117 ± 5	0.189 ± 1	0.225	0.233	0.240	1.099 ± 5
$0\bar{2}0$		0.187	1.915 ± 7	0.164 ± 1	0.227	0.234	0.241	
220	0.233	0.104	1.964 ± 7	0.170 ± 1	0.204	0.210	0.216	0.982 ± 5
$2\bar{2}0$		0.105	1.946 ± 7	0.168 ± 1	0.201	0.207	0.213	
400	0.329	0.081	1.865 ± 5	0.157 ± 1	0.177	0.181	0.185	0.852 ± 5
$0\bar{4}0$		0.151	1.775 ± 5	0.144 ± 1	0.175	0.181	0.186	
420	0.368	0.092	1.773 ± 4	0.144 ± 1	0.163	0.167	0.171	0.793 ± 5
$2\bar{4}0$		0.149	1.727 ± 5	0.138 ± 1	0.165	0.170	0.174	
440	0.466	0.124	1.581 ± 6	0.116 ± 1	0.132	0.136	0.139	0.638 ± 5
$4\bar{4}0$		0.124	1.579 ± 6	0.116 ± 1	0.132	0.135	0.139	
600	0.494	0.087	1.564 ± 6	0.113 ± 1	0.125	0.127	0.129	0.600 ± 5
$0\bar{6}0$		0.118	1.550 ± 5	0.112 ± 1	0.125	0.128	0.131	
620	0.520	0.095	1.525 ± 5	0.107 ± 1	0.118	0.120	0.123	0.572 ± 5
$2\bar{6}0$		0.127	1.518 ± 5	0.106 ± 1	0.120	0.123	0.126	
640	0.593	0.120	1.410 ± 8	0.087 ± 2	0.098	0.100	0.102	0.473 ± 13
$4\bar{6}0$		0.139	1.410 ± 7	0.087 ± 2	0.099	0.101	0.104	
800	0.658	0.098	1.372 ± 10	0.080 ± 2	0.088	0.090	0.091	0.421 ± 10
$0\bar{8}0$		0.097	1.367 ± 14	0.079 ± 3	0.087	0.089	0.090	
820	0.679	0.105	1.347 ± 11	0.076 ± 2	0.083	0.085	0.087	0.400 ± 10
$2\bar{8}0$		0.100	1.351 ± 13	0.076 ± 2	0.085	0.085	0.087	
660	0.698	0.143	1.300 ± 11	0.066 ± 2	0.075	0.077	0.079	0.370 ± 13
$6\bar{6}0$		0.141	1.313 ± 12	0.069 ± 2	0.078	0.080	0.082	
840	0.736	0.128	1.286 ± 7	0.064 ± 2	0.072	0.073	0.075	0.344 ± 14

TABLE V. Results for the polarized-beam measurements with $\vec{H} \| [0\bar{1}1]$. The columns are the same as in Table IV.

hkl	$\frac{\sin\theta}{\lambda}$	$\bar{t}$ (cm)	R_{obs}	γ_{obs}	$g=2500$ γ_{corr}	$(\mu f)_{corr}$ (μ_B)
200	0.165	0.188	1.911 ± 8	0.163 ± 2	0.232	1.092 ± 7
022 $0\bar{2}\bar{2}$	0.233	0.079	1.985 ± 5 1.984 ± 9	0.173 ± 1	0.207	0.975 ± 5
222 $\bar{2}22$	0.285	0.093	1.871 ± 6 1.874 ± 8	0.158 ± 1	0.188	0.885 ± 5
400 $\bar{4}00$	0.329	0.144	1.748 ± 7 1.750 ± 8	0.141 ± 1	0.175	0.824 ± 6
422 $\bar{4}22$	0.403	0.136	1.639 ± 6 1.646 ± 6	0.126 ± 1	0.150	0.706 ± 6
044 $0\bar{4}\bar{4}$	0.466	0.084	1.548 ± 7 1.569 ± 7	0.112 ± 2	0.126	0.593 ± 6
600 $\bar{6}00$	0.494	0.113	1.542 ± 8 1.537 ± 7	0.109 ± 1	0.126	0.593 ± 6
244 $\bar{2}44$	0.494	0.091	1.510 ± 7 1.520 ± 7	0.105 ± 1	0.119	0.560 ± 7
622 $\bar{6}22$	0.546	0.133	1.453 ± 7 1.452 ± 7	0.095 ± 1	0.110	0.518 ± 6
444 $\bar{4}44$	0.570	0.119	1.396 ± 8 1.428 ± 11	0.087 ± 2	0.100	0.471 ± 6
800 $\bar{8}00$	0.658	0.094	1.343 ± 12 1.350 ± 12	0.075 ± 2	0.085	0.400 ± 7
644 $\bar{6}44$	0.679	0.149	1.287 ± 11 1.288 ± 10	0.064 ± 2	0.075	0.353 ± 8
822 $\bar{8}22$	0.698	0.100	1.301 ± 12 1.309 ± 11	0.068 ± 2	0.076	0.358 ± 8
066 $0\bar{6}\bar{6}$	0.698	0.099	1.269 ± 11 1.264 ± 11	0.060 ± 2	0.067	0.315 ± 8
266 $\bar{2}66$	0.717	0.107	1.243 ± 11 1.244 ± 11	0.055 ± 2	0.062	0.292 ± 8

can be measured in the plane perpendicular to the applied field, and we have used the elevated counter technique.[2] In this case the square of the magnetic interaction vector q^2 is different from unity, and Eqs. (19) and (21) must be modified. The extinction corrections for these weak reflections are, of course, much smaller than for the strong reflections, but they *reduce* γ_{obs}, i.e., $R_{obs}/R_{corr} > 1$; a consequence of a γ being greater than unity. For the weak reflections the experimental form factor corrected for extinction is calculated from

$$(\mu f)_{corr} = [\gamma_{corr}(b_{Tm} - b_{Sb})/0.2696\times10^{-12}]\,\mu_B.$$

The value of γ_{corr} is clearly sensitive to the difference in the scattering amplitudes, and is given in the table as a function of b_{Tm}, assuming $b_{Sb} = 0.564\times10^{-12}$ cm. This sensitivity to b_{Tm} implies that the values of f_{corr} are uncertain unless b_{Tm} is known accurately, even though the corrections arising from extinction are small. On the other hand, the over-all agreement between f_{corr} and f_{calc} does allow us to derive a reasonable value for b_{Tm}. The best fit is obtained with $b_{Tm} = (0.697 \pm 0.005)\times10^{-12}$ cm. This measurement is independent of the unpolarized-beam result, apart from the fact that both experiments were done on the same crystal. We conclude, therefore, that the correct scattering amplitude of thulium is $(0.705 \pm 0.005)\times10^{-12}$ cm, relative to $b_{Sb} = (0.564 \pm 0.001)\times10^{-12}$ cm,[24] and we have used this value throughout.

The experimental results are given in Tables IV–VI in terms of the quantity $(\mu f)_{corr}$, where the magnetic moment μ is a constant for a given orientation, applied field, and temperature. As discussed in Sec. III an accurate measurement of the applied field is rather difficult, the estimated value lying between 12.5 and 13.0 kOe. The parameter μ may therefore be considered as a scale factor with an uncertainty of ~4%. In calculating the form factor in Eq. (1) we require the c_i coefficients and $\langle j_i \rangle$ integrals. The derivation of the coefficients is discussed in Sec. II, and the values for the two field directions given in Table VII. The $\langle j_i \rangle$ integrals are discussed in Sec. V. The best fits between the experimental and theoretical form factors are found with magnetic moment values of $(1.208 \pm 0.014)\mu_B$ and $(1.191 \pm 0.014)\mu_B$ per Tm atom in the ⟨100⟩ and ⟨110⟩ orientations, respectively. These values correspond to applied field of 12.9 ± 0.15 kOe with $\vec{H} \| \langle 100 \rangle$ and 12.5 ± 0.15 kOe with $\vec{H} \| \langle 110 \rangle$, which are within the expected range. Table VIII gives the final results for theoretical and experimental form factors for the strong (*hkl* even) reflections in both orientations. Figure 2 shows the experimental form factor in the ⟨100⟩

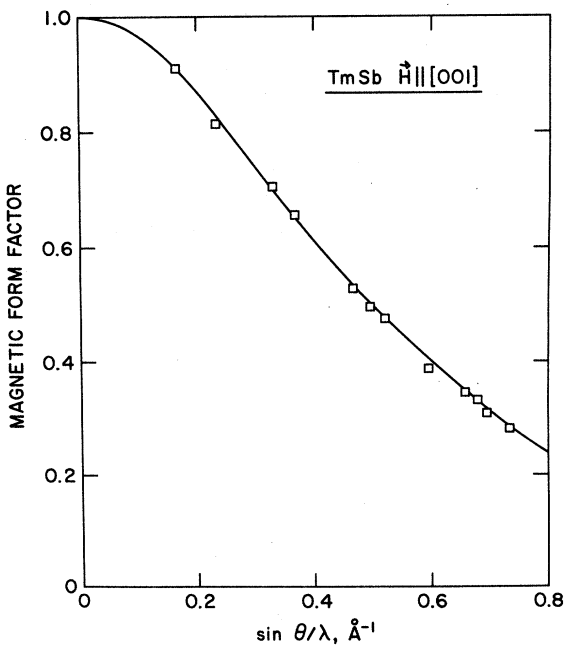

FIG. 2. The magnetic form factor of TmSb with the field applied parallel to [001]. The smooth curve is the theoretical form factor for the $M=4$ state and with $Z_4 = 2.89$ (see Sec. V). The size of the experimental points is an indication of the uncertainty in the measurements.

TABLE VI. Results for the polarized-beam measurements of the weak (*hkl* odd) reflections. q^2 is the square of the magnetic interaction vector, with $q^2=1$, $\vec{H} \parallel [0\bar{1}1]$, otherwise $\vec{H} \parallel [001]$. R_{obs}, γ_{obs}, and γ_{corr} are as in Tables IV and V. For these reflections $(\mu f)=\gamma\times(b_{Tm}-b_{Sb})/0.2696$ so that the value of f_{corr} depends strongly on $(b_{Tm}-b_{Sb})$. The three columns of f_{corr} correspond to different values of b_{Tm}, assuming $b_{Sb}=0.564$ (all $\times 10^{-12}$ cm). The last column gives f_{calc} using parameters defined in the text (see Table VIII).

	$\frac{\sin\theta}{\lambda}$	$\bar{t}$ (cm)	q^2	R_{obs}	γ_{obs}	$g=2500$ γ_{corr}	f_{corr} $b_{Tm}=0.690$	$b_{Tm}=0.705$	$b_{Tm}=0.720$	f_{calc}
$\frac{111}{1\bar{1}1}$	0.143	0.110	2/3	4.97 ± 5 4.96 ± 5	2.30 ± 2	2.24	0.867 ± 7	0.970 ± 8	1.073 ± 9	0.916
$\frac{111}{11\bar{1}}$	0.143	0.089	1.0	6.30 ± 9 6.31 ± 6	2.26 ± 2	2.21	0.867 ± 7	0.971 ± 8	1.074 ± 9	0.916
$\frac{131}{113}$	0.273	0.105	10/11	9.1 ± 5	1.85 ± 3	1.84	0.712 ± 11	0.796 ± 13	0.881 ± 15	0.752
$\frac{311}{\bar{3}11}$	0.273	0.146	1.0	9.2 ± 4 9.4 ± 3	1.91 ± 2	1.88	0.738 ± 8	0.826 ± 9	0.914 ± 11	0.755

direction over the whole angular range measured. The solid curve is the form factor for the $M=|4\rangle$ state of the Tm^{3+} ion given by $f(\bar{\kappa})=\langle j_0\rangle+0.7248\langle j_2\rangle+0.0909\langle j_4\rangle-0.0955\langle j_6\rangle$. This form factor is symmetric in the plane perpendicular to the applied field, and is very close to that expected for $\vec{H}\parallel\langle 100\rangle$, because the contribution to the cross section from the matrix elements between the $|0\rangle$ and $|\pm 4\rangle$ states is small compared to the contribution from the diagonal elements [see Eq. (18)].

Figure 3 illustrates the high-angle reflections for TmSb in the two orientations, and the same $M=|4\rangle$ form factor as in Fig. 2. The results in Table VIII, and particularly Fig. 3, indicate that the over-all agreement between theory and experiment is remarkably good.

V. WAVE FUNCTIONS

The theoretical form factors calculated in Sec. II (Table II) require an evaluation of the $\langle j_i\rangle$ integrals[30] that depends on the spatial extent of the single-electron $4f$ wave function. The first nonrelativistic Hartree–Fock (HF) calculations of these wave functions for the tripositive rare-earth ions was given by Freeman and Watson[4] (FW) in 1962. Subsequent work[31,32] restricted to nonrelativistic HF calculations has not resulted in radial distribution functions that are substantially different from those given by Freeman and Watson. The latter used a linear combination of four hydrogenic orbitals as a basis set for the radial part of the $4f$-electron wave functions.

The radial part of the wave function is given by

$$U_{4f}(r)=\sum_{i=1}^{4} C_i r^4 e^{-Z_i r}, \tag{22}$$

where the normalization condition is

$$\int_0^\infty U_{4f}^2(r)\,dr=1. \tag{23}$$

The coefficients C_i and Z_i are given in Table I

TABLE VII. Coefficients c_2, c_4, and c_6 in Eq. (1). All entries are for the scattering vector perpendicular to the applied field. Φ is the angle in degrees a direction makes with the [100] axis.

		$\vec{H}\parallel[001]$					$\vec{H}\parallel[0\bar{1}1]$		
[*hk*0]	Φ	c_2	c_4	c_6	[*hkk*]	Φ	c_2	c_4	c_6
100	0.0	0.7248	0.1450	0.1423	100	0.0	0.7241	0.1440	0.1400
410	14.0	0.7248	0.1210	0.1212					
310	18.4	0.7248	0.1060	0.1081					
					411	19.5	0.7080	0.0931	0.0168
					311	25.2	0.6978	0.0634	−0.0316
210	26.6	0.7248	0.0756	0.0814					
320	33.7	0.7248	0.0527	0.0613					
					211	35.3	0.6758	0.0072	−0.0724
					322	43.3	0.6559	−0.0357	−0.0540
					111	54.7	0.6276	−0.0826	0.0176
					122	70.5	0.5954	−0.1164	0.0952
					133	76.7	0.5870	−0.1218	0.1041
110	45.0	0.7248	0.0366	0.0472	011	90.0	0.5793	−0.1254	0.1055

of Freeman and Watson,[4] and the $\langle j_i \rangle$ integrals are obtained from

$$\langle j_i \rangle = \int_0^\infty U_{4f}^2(r) j_i(\kappa r) dr, \tag{24}$$

where $j_i(\kappa r)$ is the usual spherical Bessel function. The integrals $\langle j_i \rangle$ required for the neutron scattering cross section have been evaluated numerically for the FW radial functions by Blume, Freeman, and Watson.[30]

Before continuing to a more detailed comparison between the calculated and observed form factors, a number of general points need to be emphasized. The experiments on the rare-earth metals[1-3] indicate that the FW wave functions do not agree with experiment, except at high scattering angles, and that the $4f$ moment obtained from the high-angle data is too small. In the case of gadolinium[1] at 96 °K the $4f$ moment determined from the FW wave functions was $5.63\mu_B$, whereas magnetization data gave $6.99\mu_B$, the difference being too large to attribute to the conduction electrons. A similar situation occurs in Tm metal as well as in the present study on TmSb. The comparison between the FW wave functions and the experimental form factors suggests that the inner regions of the $4f$ radial density, which give the greatest contribution to the form factor at high scattering angles, are accurately represented by the FW nonrelativistic calculations, but the outer regions are expanded. Recent relativistic calculations[6] for both atomic Gd and Gd^{3+} are in good agreement with the experiment, and the principal effect of the relativistic treatment is the contraction of the s and p inner shells giving rise to an expansion of the $4f$ shell.[6] Relativistic calculations for Tm^{3+} are unfortunately not available at present, so we have chosen to vary the nonrelativistic FW functions to obtain agreement with the experiment. The basis set used by FW is very convenient, since the integral in Eq. (24) can be solved analytically. The solutions are

$$\begin{aligned}
\langle j_0 \rangle &= \sum_{i,j=1}^{4} N_{ij}(1 - 7X_{ij} + 7X_{ij}^2 - X_{ij}^3)/(1+X_{ij})^8, \\
\langle j_2 \rangle &= \sum_{i,j=1}^{4} N_{ij}\, 6X_{ij}(1 - \tfrac{10}{7}X_{ij} + \tfrac{5}{21}X_{ij}^2)/(1+X_{ij})^8, \\
\langle j_4 \rangle &= \sum_{i,j=1}^{4} N_{ij} \tfrac{88}{7} X_{ij}^2 (1 - \tfrac{3}{11}X_{ij})/(1+X_{ij})^8, \\
\langle j_6 \rangle &= \sum_{i,j=1}^{4} N_{ij}\, 16 X_{ij}^3/(1+X_{ij})^8,
\end{aligned} \tag{25}$$

where the normalization gives

$$\sum_{i,j=1}^{4} N_{ij} = \sum_{i,j}^{4} \frac{8! C_i C_j}{(Z_i + Z_j)^9} = 1 \tag{26}$$

and

$$X_{ij} = \left(\frac{\kappa}{Z_i + Z_j} \right)^2 .$$

TABLE VIII. Observed and calculated magnetic form factors for TmSb. The family of planes $\{hkl\}$ refers only to those with scattering vector perpendicular to $\vec{H}$ in the respective directions (see Tables IV and V).

	$\frac{\sin\theta}{\lambda}$	$\vec{H} \parallel [001]$		$\vec{H} \parallel [0\bar{1}1]$	
$\{hkl\}$		f_{corr}	f_{calc}	f_{corr}	f_{calc}
200	0.165	0.910 ± 5	0.905	0.917 ± 6	0.905
220	0.233	0.813 ± 4	0.826	0.819 ± 4	0.812
222	0.285			0.743 ± 4	0.747
400	0.329	0.706 ± 4	0.703	0.692 ± 5	0.703
420	0.368	0.657 ± 4	0.651		
422	0.403			0.594 ± 5	0.596
440	0.466	0.529 ± 4	0.529	0.498 ± 5	0.498
600	0.494	0.497 ± 4	0.502	0.498 ± 5	0.502
442	0.494			0.471 ± 6	0.468
620	0.520	0.475 ± 4	0.472		
622	0.546			0.435 ± 5	0.435
444	0.570			0.395 ± 5	0.391
640	0.593	0.388 ± 11	0.394		
800	0.658	0.347 ± 8	0.343	0.336 ± 6	0.342
820	0.679	0.331 ± 8	0.323		
644	0.679			0.297 ± 7	0.297
660	0.698	0.307 ± 11	0.301	0.265 ± 7	0.264
822	0.698			0.301 ± 7	0.301
662	0.717			0.245 ± 7	0.251
840	0.736	0.283 ± 12	0.276		

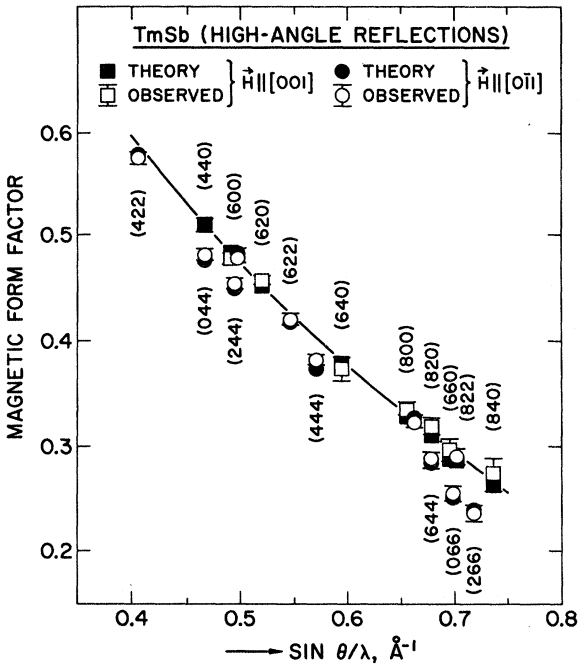

FIG. 3. The high-angle form factor for TmSb with both applied field directions. The smooth curve is the $M=4$ form factor as in Fig. 2.

Care should be taken that κ is in the same units as Z_i. If the parameters C_i and Z_i of Eq. (22) are known, the $\langle j_i \rangle$ integrals may be evaluated for a given scattering vector κ. Although in principle all eight parameters in the FW formalism could be varied in an attempt to fit the theoretical and experimental data, the high correlation between the coefficients prevents the success of such an attempt. An alternate method is based on the observation noted above that the shape of the experimental form factor at high scattering angles is identical to that derived from the FW calculations. The hydrogenic orbitals of Eq. (22) are such that their maximum in real space occurs further from the nucleus with increasing order of Z_i. The experiments suggest, therefore, that a first attempt at fitting should consider the modification of Z_4 alone, since this determines the most expanded orbital in real space. The C_i's are then renormalized and the method, if it works, is a one parameter fit. The experiments give a value for the product (μf) so a value of the magnetic moment μ must be known before the experimental and theoretical form factors can be compared. The choice of a magnetic moment is not necessarily easy, since it may lead to an unwarranted assumption about the magnetization distribution of any conduction electrons. For any choice of μ an optimum value of Z_4 may be found, although the extent of the over-all agreement between the experimental and calculated values limits the possible range of Z_4 and μ. For TmSb the uncertainty in the magnitude of the applied field introduces a corresponding uncertainty in the value of the induced magnetic moment. By varying the magnetic field, and hence the moment, we have attempted to obtain the best fit with the FW wave functions. The result of this procedure may be conveniently measured by the sum

$$s = \left(\sum_i W_i (f_{\text{corr}} - f_{\text{calc}})_i^2 \right) / n, \tag{27}$$

where $W_i = 1/\Delta f_{\text{corr}}^2$ and the sum is over all n reflections. With the FW wave functions the lowest values of s are given in Table IX and the corresponding fields are 12.5 for $\vec{H} \| \langle 100 \rangle$ and 12.1 kOe for $\vec{H} \| \langle 110 \rangle$. These values of H are low, and the fit is unsatisfactory. The Z_4 value for thulium from the FW wave functions is 3.035 (see Table I of FW). By varying Z_4 the lowest values of s are with $Z_4 = 2.90$ for the $\langle 100 \rangle$ direction with $H = 12.9$ kOe, and with $Z_4 = 2.85$ for the $\langle 110 \rangle$ direction with $H = 12.75$ kOe. The best value is then $Z_4 = 2.89$ (with an estimated error of ± 0.05) giving $\vec{H} \| \langle 100 \rangle = 12.9$ kOe and $\vec{H} \| \langle 110 \rangle = 12.5$ kOe. The least-squares residuals s are 1.60 and 1.21 in the two cases; a significant improvement over values (~ 4.5) derived with the FW wave functions.

TABLE IX. Values of the parameter Z_4, Eq. (22), and the applied field H which give the best fit [as measured by the minimum of s, Eq. (27)] between the theoretical and experimental form factors. The Freeman and Watson value is $Z_4 = 3.035$.

	Z_4	2.80	2.85	2.90	2.95	3.035
$\langle 100 \rangle$	H (kOe)	13.3	13.0	12.9	12.8	12.5
	s	4.06	2.31	1.60	2.05	4.32
$\langle 110 \rangle$	H (kOe)	12.9	12.8	12.6	12.4	12.1
	s	1.45	0.86	1.61	2.18	4.90

The above analysis, i.e., changing Z_4 to improve the agreement between the experimental and theoretical form factors, may also be applied to thulium metal, for which polarized-beam measurements have been published.[2] We first note that the experimental values of $(\mu f)_{\text{obs}}$ (see Table I of Ref. 2) are derived using a coherent nuclear scattering length of 0.69×10^{-12} cm, and that they are linearly dependent on this term. In the present experiment we have concluded that the scattering length $b_{\text{Tm}} = (0.705 \pm 0.005) \times 10^{-12}$ cm and the thulium metal $(\mu f)_{\text{obs}}$ should be correspondingly increased by 2.2%. Adjusting Z_4 and the ordered moment μ results in values of $Z_4 = 2.80$ and $\mu = 0.98 \mu_B$ per Tm atom, with $s = 1.41$. This fit is illustrated in Fig. 4, which also includes the form factor calculated with the FW value of $Z_4 (= 3.035)$. As discussed in Ref. 2, the saturation magnetization value for thulium metal is $(7.14 \pm 0.02) \mu_B$ per Tm atom, the $0.14 \mu_B$ (2%) excess over the free-ion value of $7 \mu_B$ being attributed to conduction-electron polarization. At low fields the measured moment from magnetization experiments is $(1.001 \pm 0.005) \mu_B$ per Tm atom (thulium having the 4+, 3− ferrimagnetic structure) and with a 2% conduction-electron polarization a $4f$ moment of $0.98 \mu_B$ per Tm atom would be expected, in good agreement with the analysis of the experimental data. The direct correlation between μ and b_{Tm} is such that the latter should be better determined before any great weight is attached to this agreement. The important point, however, is that the value of Z_4 is much reduced from the FW value, and shifts of 2–4% in μ and b_{Tm} result in only very minor changes (± 0.05) in Z_4. Taking into account the uncertainties in b_{Tm} and μ we estimate the error on Z_4 in thulium metal as 0.05, i.e., $Z_4 = 2.80 \pm 0.05$. Figure 4 serves to illustrate the analysis performed in Ref. 2. By scaling down the full curve (FW wave functions), i.e., adjusting b_{Tm} and μ, good agreement can be obtained with the high-angle reflections, but the low-angle reflections are then above the theoretical curve (see Fig. 2 of Ref. 2). The resulting localized moment taken from the high-angle reflections is $0.904 \mu_B$ (based on $b_{\text{Tm}} = 0.705 \times 10^{-12}$ cm), still leaving a discrepancy of

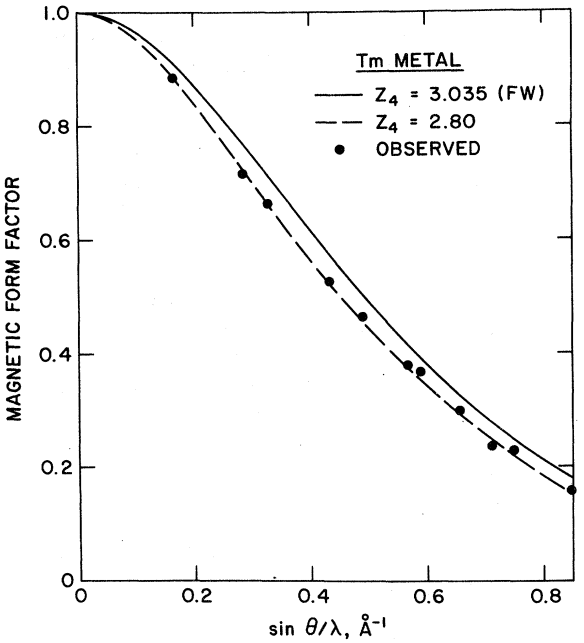

FIG. 4. The magnetic form factor for thulium metal. The smooth curve is the form factor using the Freeman and Watson nonrelativistic wave functions, the broken curve that using expanded wave functions with $Z_4 = 2.80$ (see Sec. V). The experimental points are taken from Ref. 2 using $b_{Tm} = 0.705 \times 10^{-12}$ cm and $\mu = 0.98\mu_B$ per Tm atom.

$0.1\mu_B$ between the neutron and magnetization magnetic moments. In view of this contradiction, and the evidence from gadolinium[1] and terbium[3] that the FW wave functions are definitely too contracted to account for the experimental results, we feel that the analysis with a varying Z_4 is more reliable than postulating a very large ($\sim 10\%$) conduction-electron polarization. An examination of the two lowest-angle reflections in Fig. 4 illustrates that the experimental and theoretical form factors are in agreement. In gadolinium[1] the discrepancy between experiment and the relativistic form factor at low angles leads to the assumption of a "diffuse" form factor attributed to the conduction electrons. At $\sin\theta/\lambda = 0$ the magnitude of this diffuse form factor is equal to the discrepancy between the Russell–Saunders free-ion moment gJ and the measured saturation magnetization. For gadolinium these values are $7.0\mu_B$ and $7.55\mu_B$, respectively, and for thulium they are $7.0\mu_B$ and $7.14\mu_B$. If the diffuse part of the form factor in thulium resembles that in gadolinium, the discrepancy between theory and experiment for the innermost reflection in thulium is expected to be much less than in gadolinium. In thulium metal the uncertainties in both the experimental results and in the above analysis do not allow us to draw any conclusions about a "diffuse" part of the magnetization density.

The changes in $\langle j_0 \rangle$ and $\langle j_2 \rangle$ by varying Z_4 from 3.035 (FW value) to 2.80 are shown in Fig. 5. Small changes of course also appear in $\langle j_4 \rangle$ and $\langle j_6 \rangle$ but even at the highest value of $\sin\theta/\lambda$ observed in the Tm or TmSb experiments $\langle j_4 \rangle$ and $\langle j_6 \rangle$ are only ~40 and 14% of $\langle j_2 \rangle$, respectively.

A direct consequence of the expansion of the wave functions is that the $\langle r^n \rangle$ integrals may be reevaluated.[33] These are given for thulium with $Z_4 = 3.035$ (FW value) and $Z_4 = 2.80$ (Tm metal) in Table X.

VI. DISCUSSION

From an experimental point of view the measurement of flipping ratios for TmSb at 5 °K and $H_{appl} \simeq 13$ kOe presents no special difficulties. The problem of extinction, however, has meant that relatively large ($\simeq 15\%$) corrections have been applied to the experimental data. As discussed in Sec. IV we have followed the Zachariasen method for obtaining these extinction corrections. The over-all agreement, both for equivalent reflections with different path lengths, and between theory and experiment, is a strong indication that these corrections are valid. The normal method for eliminating extinction is either to mechanically work the crystals (e.g., in the rare-earth metals) or to use very thin sections in transmission (e.g., in the iron series elements and compounds). Neither of these methods is applicable to the large class of compounds that are brittle, cleave easily, and in which single crystals are very rare, for example, TmSb. We believe, therefore, that the success in using the Zachariasen extinction correction is not only interesting in its own right, but has significance for a much wider class of compounds that could be investigated with the polarized-neutron technique.

The scatter of points about the smooth curve in Fig. 3 is very reminiscent of form-factor measurements of $3d$ transition elements and compounds, in which the scatter of points about a smooth curve is a consequence of the asymmetry in the spin density.[34–36] For the $3d$ series the crystal field potential is larger than the spin-orbit coupling, with the

TABLE X. Values of the radial expectation integrals $\langle r^n \rangle$ for thulium derived from the $4f$ wave functions. The Freeman and Watson values (Ref. 4) correspond to $Z_4 = 3.035$, and the experimental values (as deduced from the magnetic form factor) correspond to $Z_4 = 2.80$ (all in atomic units).

Z_4	$\langle r^2 \rangle$	$\langle r^4 \rangle$	$\langle r^6 \rangle$
3.035	0.65	1.06	3.67
2.80	0.83	1.97	9.33

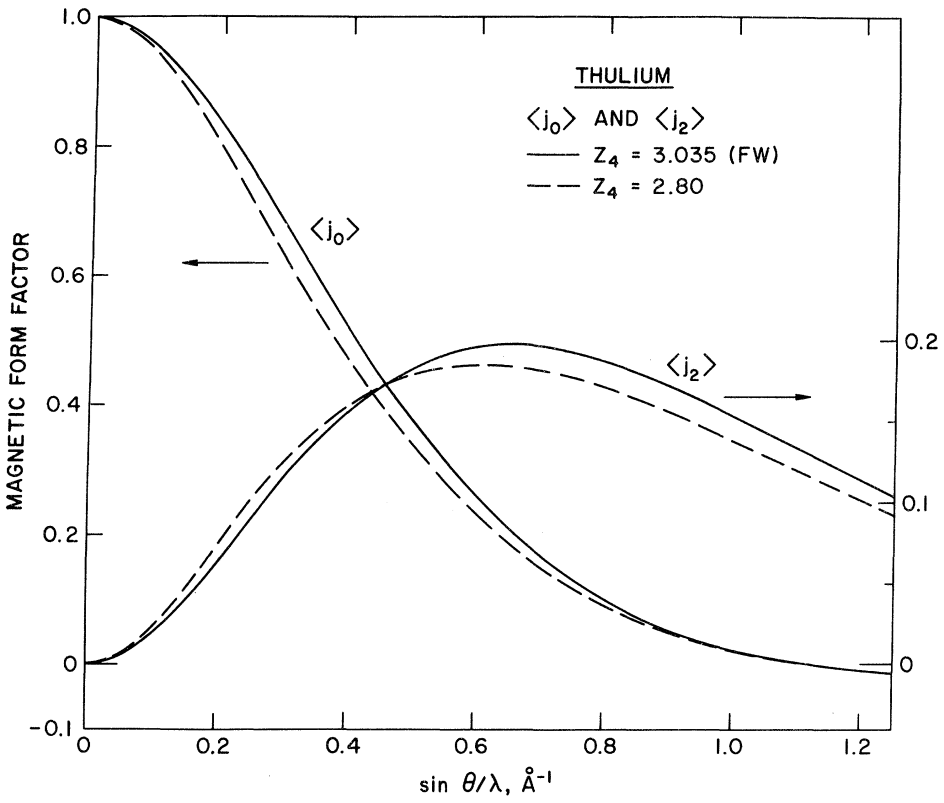

FIG. 5. The functions $\langle j_0 \rangle$ and $\langle j_2 \rangle$ derived from the FW wave functions (solid curves) and the expanded wave functions of thulium metal with $Z_4 = 2.80$ (broken curves). Note the different scales for $\langle j_0 \rangle$ and $\langle j_2 \rangle$.

result that the orbital moment is usually "quenched," and the spin direction is independent of the electron wave functions, which are constrained by the crystal symmetry. The spin density, as determined from neutron scattering experiments, is thus a function of the angle between the crystallographic axes and the scattering vector, but not of the angle between the axes and the resultant magnetic moment of the system. The spin direction is uncoupled with the spin density, and follows the applied magnetic field. A consequence of this uncoupling is that experiments on these materials are often performed with the crystal slowly rotating around the scattering vector in order to minimize multiple scattering effects.[37]

For the heavy rare-earth ions, however, the situation is quite different because the spin-orbit coupling is much stronger than the crystal field. The magnetization densities of the fully ordered heavy rare-earth metals (except gadolinium) are ellipsoids of revolution, with the direction of the magnetic moment parallel to the unique axis of the ellipsoid. This aspherical magnetization density cannot be observed with a conventional polarized-neutron experiment, in which the scattering vector is confined to the plane perpendicular to the common direction of the magnetic moment and the neutron polarization. The situation is illustrated in Fig. 6(a). The moment is along the unique axis z

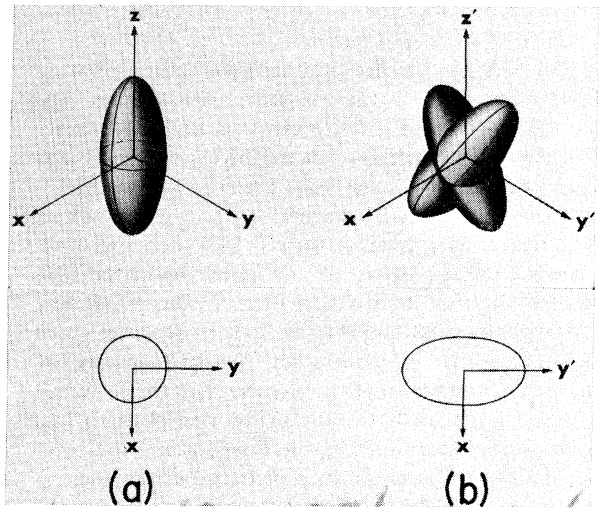

FIG. 6. Schematic representation of the magnetization density for the two field directions in TmSb. On the left (a) with $\vec{H} \parallel \vec{Z}$ the situation corresponds to $\vec{H} \parallel [001]$. The over-all density is anisotropic, but the projection onto the xy plane is a circle and gives rise to a form factor with no directional dependence in the xy plane. On the right (b) with $\vec{H} \parallel \vec{Z}'$ the system has been rotated 45° so that $\vec{H} \parallel [0\bar{1}1]$. The magnetization density may be viewed as the resultant of two lobes constrained by the crystal field along the nearest cube edges. The projection onto the xy' plane is then an ellipse, giving rise to a Φ dependence in the form factor.

of the ellipsoid. The projection of the magnetization density onto the xy plane is a circle, and measurements in this plane give no information on the over-all asphericity of the density. To observe the aspherical nature of the magnetization density the normal-beam technique, in which measurements are taken out of the xy plane, must be used. Such measurements have been reported for thulium metal.[2] A consequence of the strong LS coupling in the saturated heavy rare-earth ions is that the direction of the magnetic moment is also the unique axis of the ellipsoid. Therefore, in a form factor study on a fully ordered rare-earth ion, no additional information can be obtained by aligning the magnetic moments in more than one crystallographic direction.

To study the effect of the crystal field on the magnetization density a nonsaturated ion must be chosen. The present experiment on the induced moment in a paramagnetic system is a good example. In some senses the low-field properties of TmSb are opposite to those of the fully ordered metals, since in TmSb the magnitude of the induced moment is independent of the field direction, whereas the magnetic form factor depends on the angle the crystallographic axes make with both the scattering vector and the moment direction. The magnetization density in TmSb for the two field directions is drawn schematically in Fig. 6. For $\vec{H} \| [001]$ the density resembles that calculated for a free thulium ion in the $M = 4$ state, and is shown in Fig. 6(a). (The asphericity is greatly exaggerated.) The magnetization density for $\vec{H} \| [0\bar{1}1]$ is illustrated in Fig. 6(b). The system has been rotated about the x axis so that the field is in the $[0\bar{1}1]$ direction. The resultant J vector is parallel to the field, as LS coupling requires for an isotropic system, but the magnetization density is constrained by the crystal symmetry, and may be viewed as the resultant of two axially symmetric densities. The projection of this density on the xy' plane (i.e., perpendicular to the applied field) is then an ellipse. The change in the magnetization density as a function of the applied-field direction leads to an interesting experimental effect. If we measure the (660) reflection with $\vec{H} \| [001]$, the calculated form factor is 0.301. By rotating the crystal about the scattering vector until $\vec{H} \| [0\bar{1}1]$, the induced moment remains the same, but the (660) form factor is reduced to 0.264. The experimental confirmation of the Φ anisotropy is illustrated in Fig. 3, and the theoretical and observed values for the magnetic form factor are in complete agreement. Note that if we had chosen an $(h00)$ reflection the form factor would have been almost independent of the field direction. In the limit of infinite field, the form factor anisotropy, as measured in this experiment, would tend to disappear (since the ground state tends toward the fully ordered state), whereas the anisotropy of the bulk magnetization increases.

The variation of the magnetic form factor with the direction of the applied magnetic field is a result of the crystal field interaction. Clearly, the present technique may be applied to the problem of determining the ground state in the many materials that are not as well understood as TmSb. The method may also be used with ordered systems, in which the exchange rather than the applied field must be considered. Uranium dioxide is a good example of such a problem, and the measured form factor[38] exhibits considerable scatter about a smooth curve.

The expansion of the single-electron $4f$ radial wave functions, relative to the nonrelativistic calculations of FW, has been discussed in Sec. V. Within our experimental uncertainties the spatial extent of the $4f$ electrons in TmSb is the same as that derived from the polarized-neutron study of thulium metal.[2] These radial wave functions are, however, considerably expanded as compared to those of FW, and we attribute this difference to relativistic effects.[5,6] The $\langle r^n \rangle$ radial integrals may then be reevaluated (Table X), and the absolute value of the crystal field parameters examined. From Eqs. (9) and (16),

$$A_4^0 \langle r^4 \rangle = 82.9\ ^\circ\mathrm{K} \quad \text{and} \quad A_6^0 \langle r^6 \rangle = 4.8\ ^\circ\mathrm{K}. \tag{28}$$

The point-charge estimates of A_4^0 and A_6^0 are given by Eq. (10) and are

$$\begin{aligned} A_4^0 \langle r^4 \rangle &= 21.7 \langle r^4 \rangle Z\ ^\circ\mathrm{K}, \\ A_6^0 \langle r^6 \rangle &= 0.07 \langle r^6 \rangle Z\ ^\circ\mathrm{K}, \end{aligned} \tag{29}$$

where $\langle r^n \rangle$ are in atomic units, and Z is the effective charge on neighboring ions. From (28) and (29) we have

$$\langle r^4 \rangle Z^{(4)} = 3.8, \quad \langle r^6 \rangle Z^{(6)} = 68.6.$$

Using the $\langle r^n \rangle$ values in Table X for the FW wave functions the effective charges from the two terms are $Z^{(4)} \simeq 3.6$, and $Z^{(6)} \simeq 19$. With the experimental $\langle r^n \rangle$ integrals $Z^{(4)} \simeq 2$ and $Z^{(6)} \simeq 7$. Birgeneau *et al.*[9] have argued that the simple point-charge model is at best qualitatively correct for TmSb, and the fact that $Z^{(4)}$ (derived with the FW wave functions) lies outside the range $2 < Z < 3$ indicates that the conduction electrons are not as effective in shielding the crystal field as expected. The present experiment significantly improves on their conclusions. Crystal field spectroscopy yields a value for the product $A_n^0 \langle r^n \rangle$, but the polarized-neutron experiments give an indication of the $\langle r^n \rangle$ integrals separately. The result, as we have seen, is that the agreement between the simple point-charge model in TmSb is even better than Birgeneau *et al.* had realized. The sixth-order term is still larger than the theory predicts, but by reevaluating $\langle r^6 \rangle$

we have decreased the discrepancy from a factor of 10 to about $3\frac{1}{2}$, which, in view of the small absolute value of this term, is very reasonable.

ACKNOWLEDGMENTS

We would like to thank I. S. Jacobs and B. R. Cooper for the loan of the single crystals and their encouragement. We are grateful to R. C. Maglic, R. L. Hitterman, and H. W. Knott for valuable experimental assistance, and to F. Pinski for help with the computations. It is a pleasure to thank A. J. Freeman for many informative discussions, and G. Felcher for providing us with the analytical evaluation of the $\langle j_i \rangle$ functions given in Eq. (25).

---

†Work performed under the auspices of the U. S. Atomic Energy Commission.

[1]R. M. Moon, W. C. Koehler, J. W. Cable, and H. R. Child, Phys. Rev. B 5, 997 (1972).

[2]T. O. Brun and G. H. Lander, Phys. Rev. Letters 23, 1295 (1969).

[3]T. O. Brun and G. H. Lander, J. Phys. (Paris) 32, C1-571 (1971).

[4]A. J. Freeman and R. E. Watson, Phys. Rev. 127, 2058 (1962).

[5]H. L. Davis and J. F. Cooke, in *Magnetism and Magnetic Materials*, edited by C. D. Graham, Jr. and J. J. Rhyne (AIP, New York, 1972), p. 1441.

[6]J. P. Desclaux and A. J. Freeman, Bull. Am. Phys. Soc. 17, 269 (1972); Int. J. Magnetism 3, (1972).

[7]B. R. Cooper and O. Vogt, Phys. Rev. B 1, 1211 (1970).

[8]S. Foner, B. R. Cooper, and O. Vogt, Phys. Rev. B 6, 2040 (1972).

[9]R. J. Birgeneau, E. Bucher, L. Passell, and K. C. Turberfield, Phys. Rev. B 4, 718 (1971).

[10]G. T. Trammell, Phys. Rev. 92, 1387 (1953).

[11]D. F. Johnston, Proc. Phys. Soc. (London) 88, 37 (1966).

[12]S. W. Lovesey and D. E. Rimmer, Rept. Progr. Phys. (London) 32, 333 (1969).

[13]T. O. Brun and G. H. Lander, Phys. Rev. Letters 29, 1172 (1972).

[14]E. Balcar, S. W. Lovesey, and F. A. Wedgwood, J. Phys. C 3, 1292 (1970).

[15]G. H. Lander and T. O. Brun, J. Chem. Phys. 53, 1387 (1970).

[16]K. R. Lea, M. J. M. Leask, and W. P. Wolf, J. Phys. Chem. Solids 23, 1381 (1962).

[17]M. T. Hutchings, in *Solid State Physics*, edited by F. Seitz and D. Turnbull (Academic, New York, 1964), Vol. 16, pp. 227–273.

[18]B. G. Wybourne, in *Spectroscopic Properties of Rare Earths* (Interscience, New York, 1965), p. 163. Some of the entries in Table 6.1 of this book are incorrect. A corrected table of the relationships between the B_q^k's of the tensor-operator technique and the A_m^n of the operator-equivalent method has been given by A. J. Kassman, J. Chem. Phys. 53, 4118 (1970).

[19]A. R. Edmonds, in *Angular Momentum in Quantum Mechanics* (Princeton U. P., Princeton, N. J., 1957).

[20]S. A. Marshall, in *Optical Properties of Solids* (Plenum, New York, 1969), p. 515. In Table XV of this reference the element $D^4(0, \frac{1}{2}\pi, 0)_{2,3}$ should be $+\frac{1}{8}\sqrt{14}$.

[21]A. Messiah, *Quantum Mechanics II* (North-Holland, Amsterdam, 1964).

[22]C. W. Nielson and G. F. Koster, *Spectroscopic Coeffcients for the p^n, d^n, and f^n Configurations* (MIT, Cambridge, Mass., 1963).

[23]A. Atoji, J. Chem. Phys. 52, 6431 (1970).

[24]C. G. Shull (private communication).

[25]W. H. Zachariasen, Acta Cryst. 23, 558 (1967).

[26]P. Coppens and W. C. Hamilton, Acta Cryst. A 26, 71 (1970).

[27]M. J. Cooper and K. D. Rouse, Acta Cryst. A 26, 214 (1970).

[28]W. Stutius (private communication).

[29]W. C. Koehler, J. W. Cable, E. O. Wollan, and M. K. Wilkinson, Phys. Rev. 126, 1672 (1962).

[30]M. Blume, A. J. Freeman, and R. E. Watson, J. Chem. Phys. 37, 1245 (1962).

[31]J. B. Mann, Los Alamos Scientific Laboratory Report No. LA3691, 1968 (unpublished).

[32]M. Synek and W. Timmons, Phys. Rev. 185, 38 (1969).

[33]T. O. Brun, G. H. Lander, and G. P. Felcher, Bull. Am. Phys. Soc. 16, 325 (1971).

[34]C. G. Shull and H. A. Mook, Phys. Rev. Letters 16, 1 (1966).

[35]H. A. Mook, Phys. Rev. 148, 495 (1966).

[36]P. D. DeCicco and A. Kitz, Phys. Rev. 162, 486 (1967).

[37]R. M. Moon and C. G. Shull, Acta Cryst. 17, 805 (1964).

[38]B. C. Frazer, G. Shirane, D. E. Cox, and C. E. Olsen, Phys. Rev. 140, A1448 (1965).

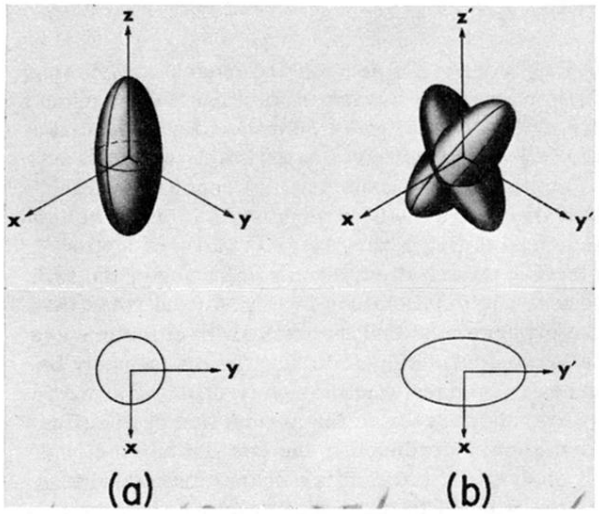

FIG. 6. Schematic representation of the magnetization density for the two field directions in TmSb. On the left (a) with $\vec{H} \parallel \vec{Z}$ the situation corresponds to $\vec{H} \parallel [001]$. The over-all density is anisotropic, but the projection onto the xy plane is a circle and gives rise to a form factor with no directional dependence in the xy plane. On the right (b) with $\vec{H} \parallel \vec{Z}'$ the system has been rotated 45° so that $\vec{H} \parallel [0\bar{1}1]$. The magnetization density may be viewed as the resultant of two lobes constrained by the crystal field along the nearest cube edges. The projection onto the xy' plane is then an ellipse, giving rise to a Φ dependence in the form factor.